


Carbon precipitation on the bonding line between deposited material and base material using an additive manufacturing process

 <https://doi.org/10.56238/sevned2024.018-048>

Henrique Cechinel Casagrande¹, Anderson Daleffe², Gilson de March³, Carlos Antônio Ferreira⁴, Joélson Vieira da Silva⁵, Hadrian Martins⁶, Lirio Schaeffer⁷, Jovani Castelan⁸ and Daniel Fritzen⁹

ABSTRACT

The additive manufacturing (AM) technique creates parts from successive deposition of material layer by layer. What makes this process a great industrial power is the savings in raw materials, compared to other types of manufacturing processes, as well as the manufacture of complex or customized parts, which other techniques would not be able to meet, or would depend on complementary processes. However, when dealing with metal MA, more precisely the method using the electric arc, high temperatures are required for wire fusion, generating heat transfers between the materials. Thus, this study seeks to understand the influence of temperature on the behavior of carbon precipitation on the contact surface between the base plate and the layers of material deposited by this process. Two consumables were evaluated, AWS A5.18 ER70S-6, and AWS A5.20 E71T-1C wire. For mechanical characterization, a Vickers microhardness test was performed, and for structural evaluation, metallographic analyses were performed. After the microhardness test, an increase in hardness on the outside of the wall of 11 % was found for the E71T-1C wire, and 17 % for the ER70S-6 wire, however, for the E71T-1C material, this value was maintained with a layer of up to 0.3 millimeters, while for the ER70S-6 material, this layer was 0.1 millimeters. The metallographic evaluation showed carbon precipitation from the base material to the added material, as well as the appearance of dendrites and Widmanstätten ferrite in the deposited metals.

Keywords: Additive Manufacturing, ER70S-6 Wire, E71T-1C Wire, SAE 1020.

¹ UNISATC

² UNISATC

³ UNISATC

⁴ UNISATC

⁵ UNISATC

⁶ UNISATC

⁷ UFRGS

⁸ UNISATC

⁹ UNISATC



INTRODUCTION

The understanding of metallurgical characteristics is necessary when there is a need for dimensioning for structural projects, automotive or aeronautical industry, where manufacturing error must be mitigated, or even in the space industry, where components with high mechanical strength and with the lowest possible weight are required.

Thus, additive manufacturing has been used for the manufacture of complex components, which compared to other manufacturing processes can improve production time, providing a rapid creation of a basic model, or a prototype from which other models and the product itself in its final version will be obtained [1][2][3]. In addition, other notable characteristics can be mentioned, such as the level of detail and the use of more than one material in the construction [4].

Even with these benefits, parts produced by this technique typically require machining to meet dimensional tolerances and surface finish. However, even with the additional machining step, additive manufacturing remains a more economical alternative to fully subtractive machining, given the lower material disposal [5].

In this type of printing technique, when starting the process, a base metal plate is usually used to support the first layer. Normally, this base has similar characteristics to the deposition material, however, it is important to understand the influence of the base metal on the first deposited layers. Thus, this work investigates the influence of the thermal exchange of the medium and the printed product and analyzes the carbon precipitation of the base metal to the deposited material.

For the analysis of the metallographic characteristics, an optical microscope was used and the mechanical evaluations were performed using the results of Vickers microhardness. However, to understand the chemical composition present in each material, the optical emission spectrometry technique was used.

THEORETICAL FRAMEWORK

ADDITIVE MANUFACTURING

Additive manufacturing (AM), commonly known as 3D printing, is a rapidly evolving technology with significant advances in the field of manufacturing processes, transforming the concepts of production lines in various industries. The American Society for Testing and Materials (ASTM) has defined AM as "a constituent linking procedure to generate things from 3D model statistics, typically layer upon layer, as divergent from subtractive engineering procedures" [6].

Emerging in the mid-1980s, AM has become a cutting-edge technology that has driven the latest industrial transformation. Based on the principle of layer-by-layer construction of three-dimensional (3D) structures directly from computer-aided design (CAD) models. AM techniques

offer several advantages, including design customization, minimal use of tools, and the ability to manufacture more technically complex products. [7, 8].

WAAM

Arc flash additive manufacturing (WAAM) is an additive manufacturing process that uses an arc flash as a heat source to melt metal feed wire and deposit it into desired 3D shapes [9].

WAAM manufacturing allows the construction of elements on a large scale, relatively quickly and economically, suitable for the construction sector where cost is a key point. Despite the potential of this new technology, the fundamental properties of WAAM materials remain elusive [10].

ARAME AWS A5.18 ER70S-6

The wire used to manufacture the samples was ER70S-6. This, in turn, has a low carbon content, which is around 0.08% by weight. Usually, this material is used for the manufacture of metal structures and general use in metallurgy, due to its affordable cost compared to other materials [11].

Table 1 shows the chemical composition according to the standard.

Table 1: Chemical Composition of AWS A5.18 ER70S-6 Wire

C (%)	Mn (%)	Si (%)	P (%)	S (%)	Ni (%)	V (%)	Cr (%)	Mo (%)	Cu (%)
0,06	0,04	0,80	0,025	0,035	0,15	0,03	0,15	0,15	0,5
0,15	0,85	1,15	Max	Max	Max	Max	Max	Max	Max

Source: [11].

ARAME AWS A5.20 E71T-1C

AWS A5.20 E71T-1C wire is suitable for welding structures made of carbon steel and low-alloy structural steel with tensile strength greater than or equal to 490MPa. It also has widespread application in the marine industry, mechanics and pressure vessels, low and medium carbon steels, heavy construction, and maintenance workshops. This wire offers an excellent deposition rate, stable arc for a superior bead finish, low spatter index, and easy slag removal, providing efficiency and yield in operation [12]. Table 2 shows the chemical composition according to the standard.

Table 2: Chemical Composition of AWS A5.20 E71T-1C Wire

C (%)	Mn (%)	Si (%)	P (%)	S (%)	Ni (%)	V (%)	Cr (%)	Mo (%)	Cu (%)
0,12	1,75	0,90	0,030	0,030	0,50	0,08	0,20	0,30	0,35
Max.	Max.	Max.	Max.	Max.	Max.	Max.	Max.	Max.	Max.

Source: [12].

SAE 1020 STEEL

SAE 1020 steel was used as a substrate or base material. This material is considered low carbon and is commonly used in the metalworking industry due to its ductility, machinability, and

weldability characteristics. The main applications are in the automotive, railway, naval, civil construction, and aeronautical industries, as well as in the manufacture of sheets and tubes [13] [14].

METHODS

Next, it will present how this study was carried out, the materials used, and tests for chemical and mechanical characterization.

OPTICAL EMISSION SPECTROMETRY

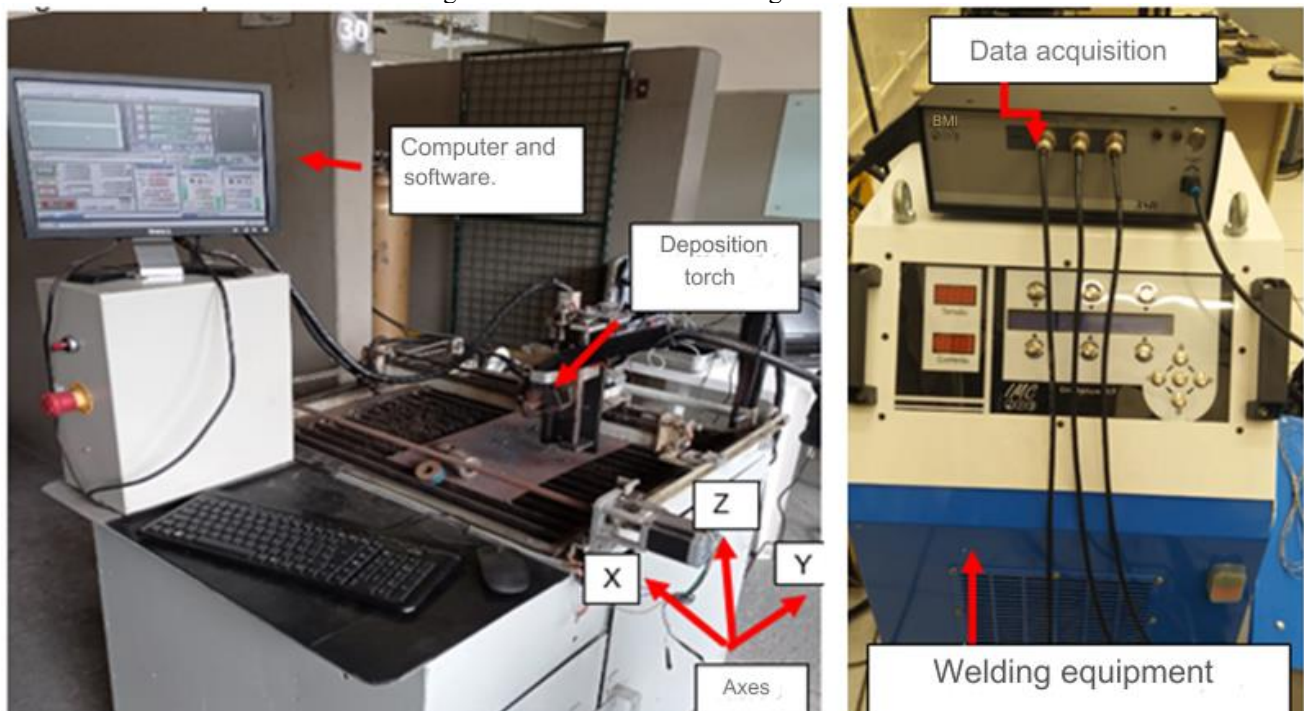
For the chemical determination of the wire, the optical emission spectrometry test was performed. The equipment used was a spectrometer from the manufacturer BRUKER, model Q2 ION. The power used was 400 Watts for 30 seconds. The triplicate test is highlighted to validate the method.

ADDITIVE MANUFACTURING MACHINE

To print the samples, a welding machine from the manufacturer IMC model DIGIplus A7 was used, linked to the SAP 3SR data acquisition device.

Figure 1 details the additive manufacturing equipment, the device with CNC coordinates, and the welding machine.

Figure 1: Additive Manufacturing Machine



Source: From the author (2024).



As can be seen in Figure 1, the equipment has movement in three axes, X, Y, and Z, longitudinal and vertical transverse, respectively. Programming is carried out through the MACH 3® software, in programming language G. However, the welding equipment has a data acquisition tool for voltage (V), current (A), wire-speed (m/min.), gas flow (L/min.), and power (W) among other parameters.

METALLOGRAPHY TESTING

An Olympus SC30 microscope was used to analyze the constituents according to ABNT NBR 15454. The acid used to reveal the phases present in the metal was vital at 2% for 10 seconds.

VICKERS MICROHARDNESS TEST

The Vickers microhardness test in profile was performed for mechanical evaluation. For this purpose, a SHIMADZE® microhardness tester, model HMV-2TADW, was used. The applied load was 4.903 Newtons with an application time of 10 seconds for the sample nucleus. The first indentation was performed at the end of the welded wall, using a load of 2.943 Newtons, according to the ABNT NBR NM ISO 6507 standard.

BASE MATERIAL

To present characteristics compatible with the wires under study, SAE 1020 steel was adopted as the base metal. The sheet has the following dimensions; 150 x 75 x 6.35 mm. The use of optical emission spectrometry, as described in item 2.1 for chemical characterization, is noteworthy.

RESULTS

SPECTROMETRY FOR SAE 1020 STEEL AND ER70S-6 AND E71T-1 WIRES

As shown in Table 3, the carbon content for both materials is similar, which justifies the application of the SAE 1020 base material.

Table 3: Chemical composition ER70S-6 and SAE 1020.

Element	ER70S-6 (%)	SAE 1020 (%)	E71T-1C (%)
Carbon (C)	0,104	0,107	0,063
Silicon (Si)	0,657	<0,0050	0,649
Manganês (Mn)	1,259	0,465	1,443
Phosphorus (P)	0,014	0,016	0,0051
Sulphur (S)	0,010	<0,0030	0,0057
Chromium (Cr)	0,020	0,020	0,027
Molibdênio (Mo)	0,014	0,0096	0,014
Copper (Cu)	0,093	0,0045	0,0067
Iron (Fe)	Ball.	Ball.	Ball.

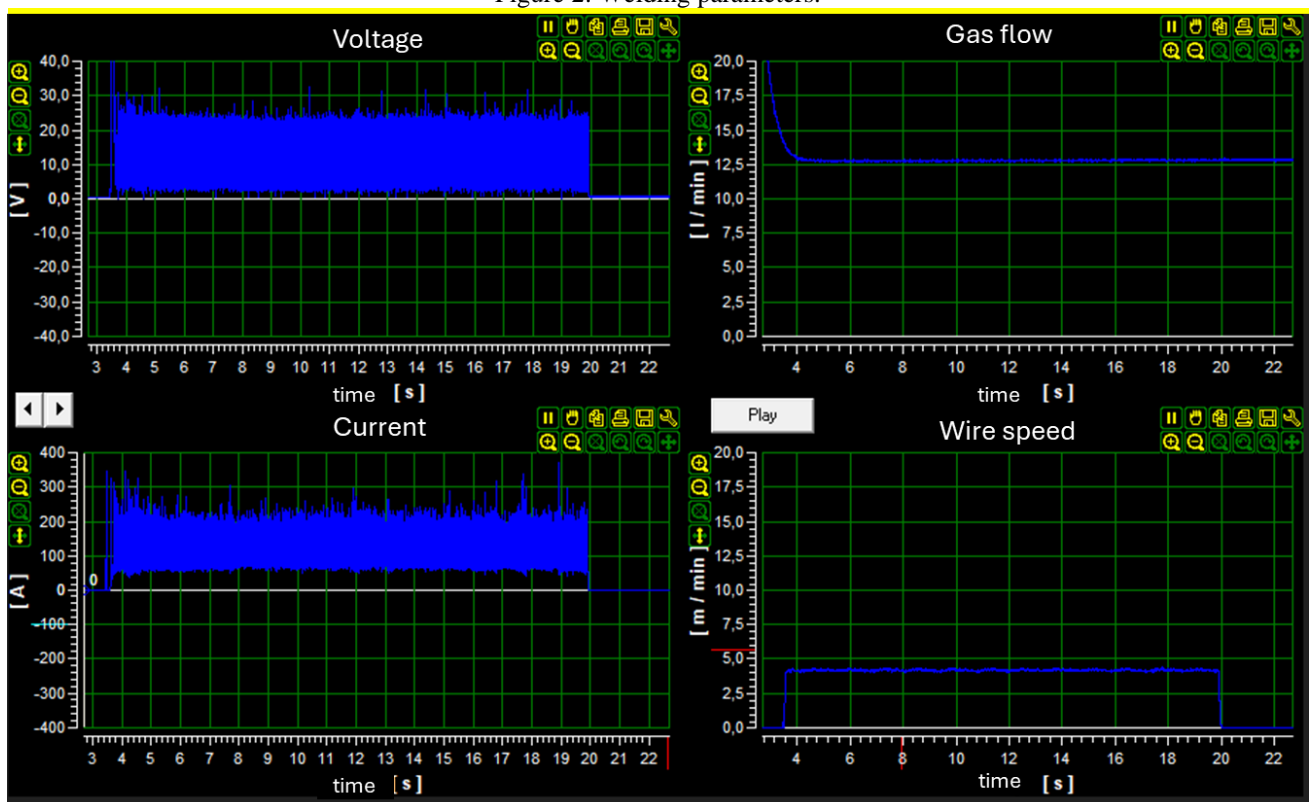
Source: From the author (2024).

Other components are part of the structure of these materials, especially the use of manganese as a deoxidizer and desulfurizer. When manganese is present in concentrations below 1%, it does not negatively affect weldability, although it can increase the hardness of the material. At concentrations greater than 1 %, manganese can increase the propensity to crack during the welding process. [15] [16] [17].

SAMPLES MANUFACTURED BY ADDITIVE MANUFACTURING

First, the parameters of the wire in question were adjusted. Figure 2 details the parameters used to manufacture the samples.

Figure 2: Welding parameters.



Source: From the author (2024).

The mean for the welding parameters are presented in Table 4.

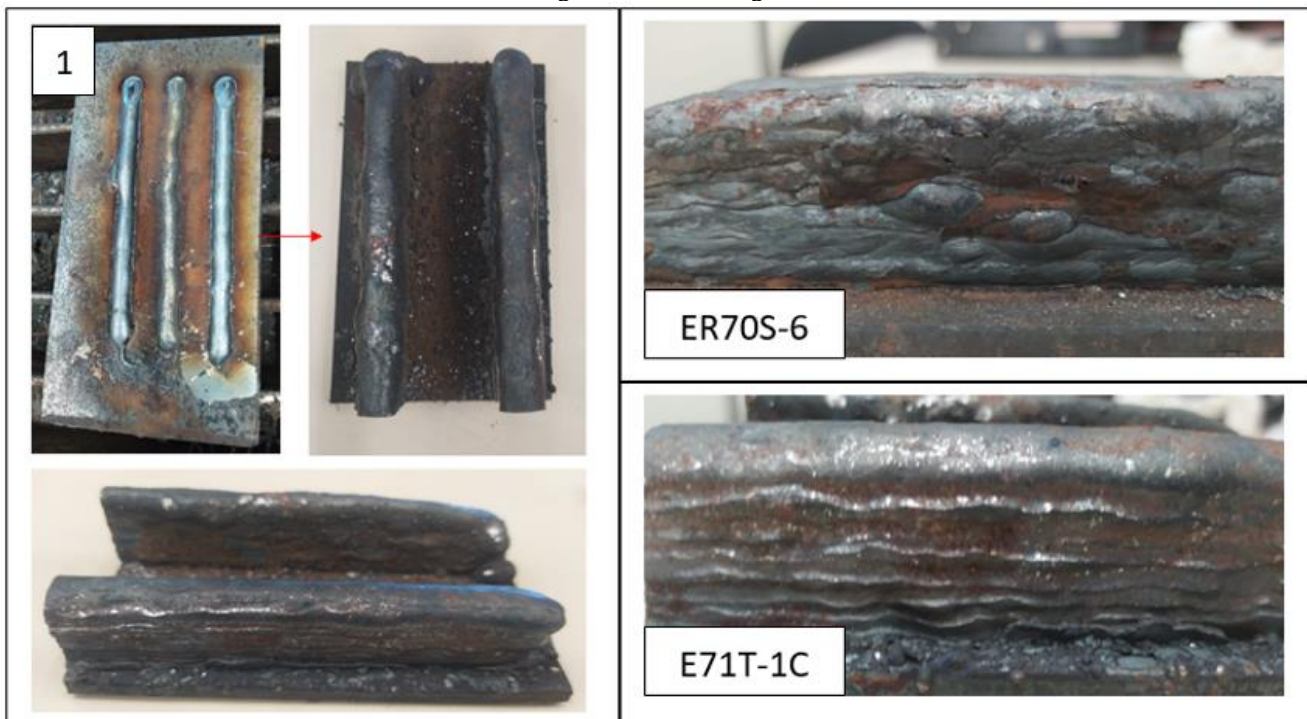
Table 4: Welding parameters.

Parameter:	ER70S-6:E71T-1C:	
Current (A)	131	168
Voltage (V)	18,2	19,9
Gas flow rate (L/min.)	12,3	13,4
Wire speed (m/min.)	4,8	6,1
Argon (%)	85	85
Carbon dioxide (%)	15	15
CNC Displacement (mm/min.)	300	300

Source: From the author (2024).

The manufactured wall is approximately 130 mm long, 25 mm high, and 12 mm thick. The impression was performed with a double cord laterally. The increment for each pass, i.e., the value that the machine shifted vertically to each layer, was approximately 2.8 mm, totaling 9 layers. Figure 3 shows the sequence of sample production, which begins with the adjustment of the parameters (1) until the final print.

Figure 3: 3D Printing



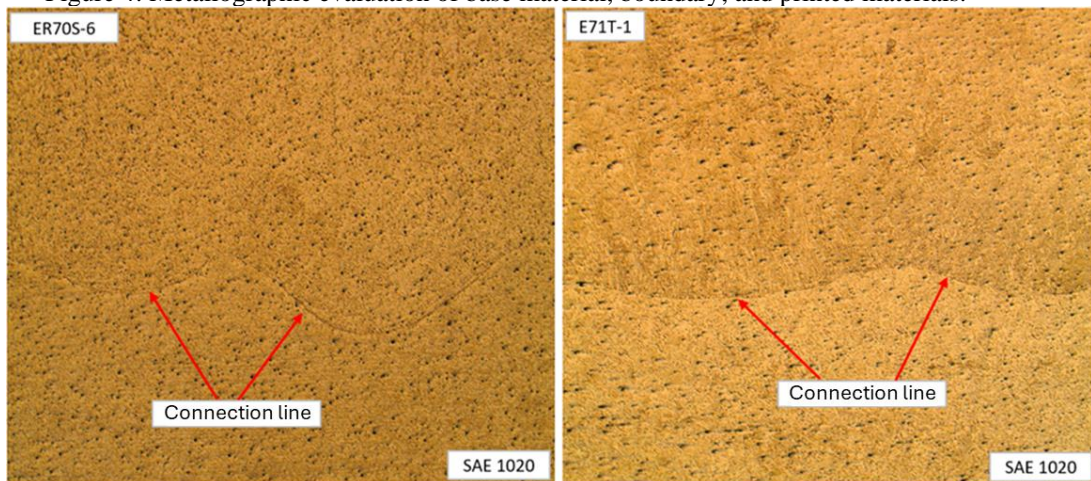
Source: From the author (2024).

After the fabrication of the samples, they were cut and ground on a band saw from the manufacturer Franho model FM 18S and a flat grinding machine from the manufacturer Mello model P36, respectively.

METALLOGRAPHIC TESTING

Figure 4 shows the connection zone between the SAE 1020 steel base metal plate and the materials printed by additive manufacturing. In the twelve-fold magnification image, it is possible to observe that for ER70S-6 wire, penetration into the base metal was greater, however, for E71T-1C wire the penetration was reduced. This phenomenon is because the chemical elements present in SAE 1020 steel and ER70S-6 wire have closer contents, compared to E71T-1C wire, thus explaining the equivalent penetration values.

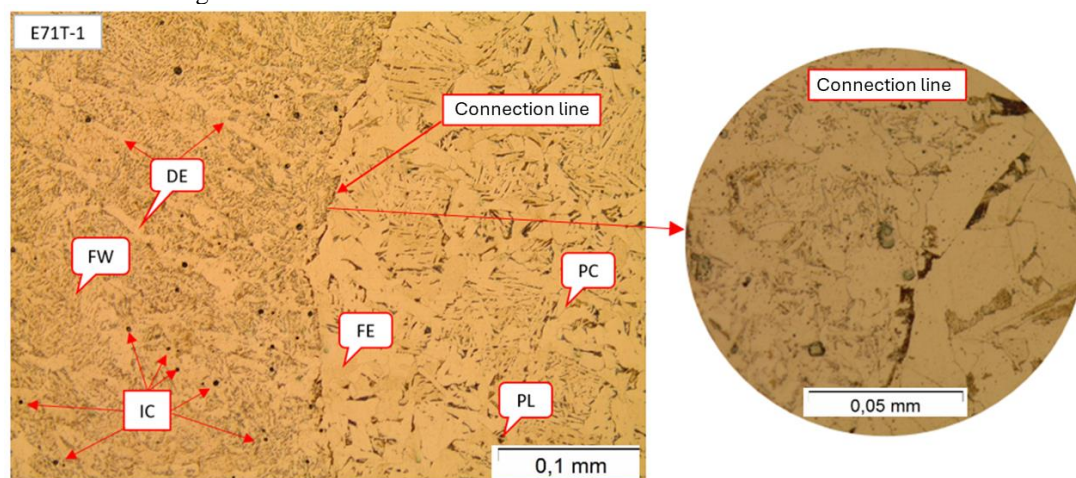
Figure 4: Metallographic evaluation of base material, boundary, and printed materials.



Source: From the author (2024).

Figure 5 shows in detail the structures for the base plate, contact surface, and deposited material. The following elements can be observed: Ferrite (FE), Perlite (PL), Grain Boundary Perlite (PC), Inclusion (IC), Dendrite (DE), and Widmanstätten Ferrite (FW).

Figure 5: Contact surface between SAE 1020 steel and E71T-1C wire.

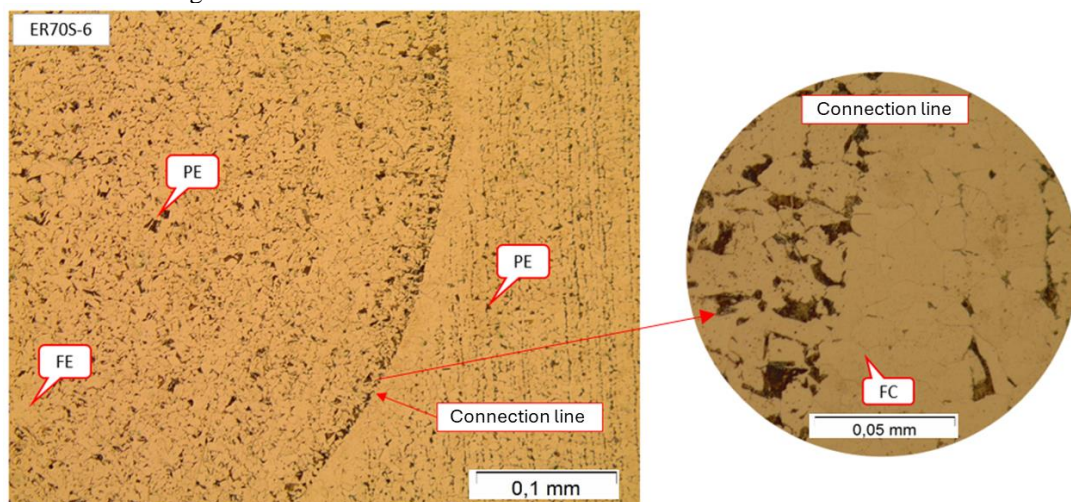


Source: From the author (2024).

It can be seen in Figure 5 that the base material (SAE 1020) is composed of the microstructure ferrite and the microconstituent pearlite, however, ferrite is predominant in the matrix because it is low-carbon steel. However, on the bond line, it is possible to visualize the carbon precipitation from the base metal to the welded metal. In the case of the deposited material E71T-1C, it presented a significant amount of pores during the printing process. According to Duarte et al (2024), when there is a subsequent layer of welding such as AM, the material recrystallizes, however, due to the high temperatures, residual stresses and inclusions are present in the printed samples [18]. The material deposited in the first layer has dendrites, caused by the rapid cooling process, as well as Widmanstätten ferrite, characteristic of the welding process.

Figure 6 details the metallography for ER70S-6 wire, where this material demonstrated carbon precipitation to the contact surface. However, it has a similar structure compared to the base material, since the material deposition region is composed of the ferrite phase and the microconstituent perlite.

Figure 6: Connection line between SAE 1020 steel and ER70S-6 wire.



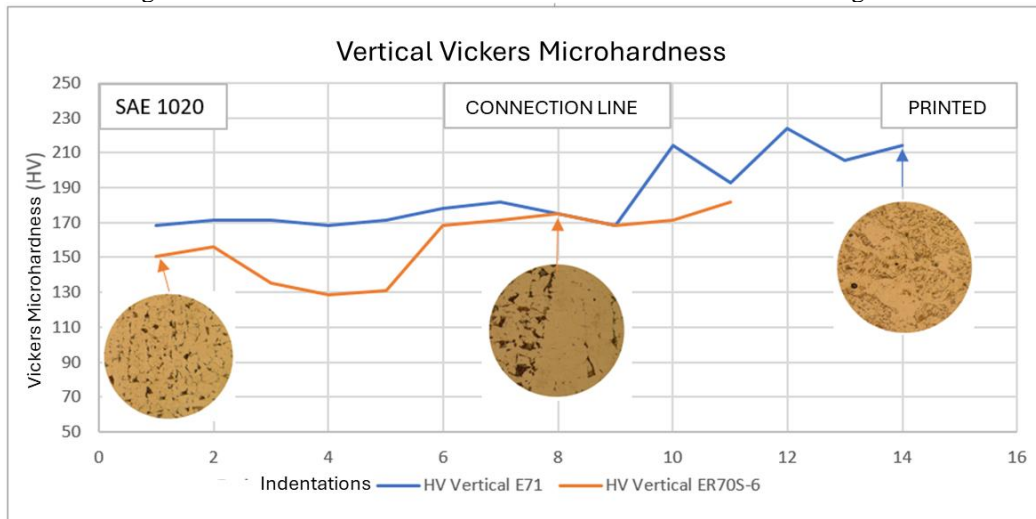
Source: From the author (2024).

A greater amount of ferrite is observed in the connection line, due to the carbon precipitation for the deposited material, and thus the grain boundary ferrite stands out, as shown in Figure 6.

VICKERS MICROHARDNESS TEST

Figure 7 shows the results pertinent to the microhardness evaluation. In this test, the measurements started in the base material (SAE 1020), presenting a microhardness of 150 and 169 HV. For the bonding region, the microhardness was measured with approximately 175 HV. When arriving at the printed material, the value for E71T-1C wire was up to 224 HV, and for ER70S-6 wire 182 HV.

Figure 7: Microhardness SAE 1020 steel and Additive Manufacturing wires.

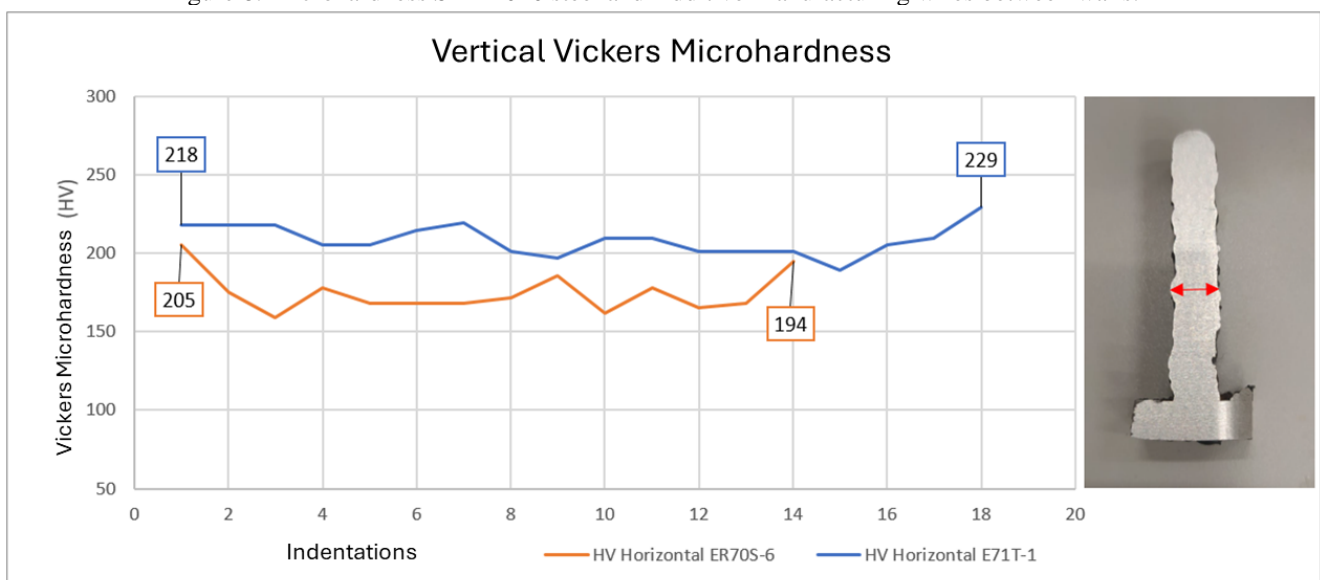


Source: From the author (2024).

Figure 8 shows the results for Vickers microhardness perpendicular to the deposition. The objective is to evaluate the hardness between the ends and the core of the deposition and to evaluate the effects of thermal exchange with the external environment.

In the graph, it is evident that the first indentation at a distance of 0.1 millimeter from the end, has greater hardness, as shown in Figure 8. For the ER70S-6 material, the first measurement at the left and right ends was 205 and 194 HV, respectively. However, after the first measurement, the microhardness is reduced and remains at an average of 171 HV \pm 7.

Figure 8: Microhardness SAE 1020 steel and Additive Manufacturing wires between walls.

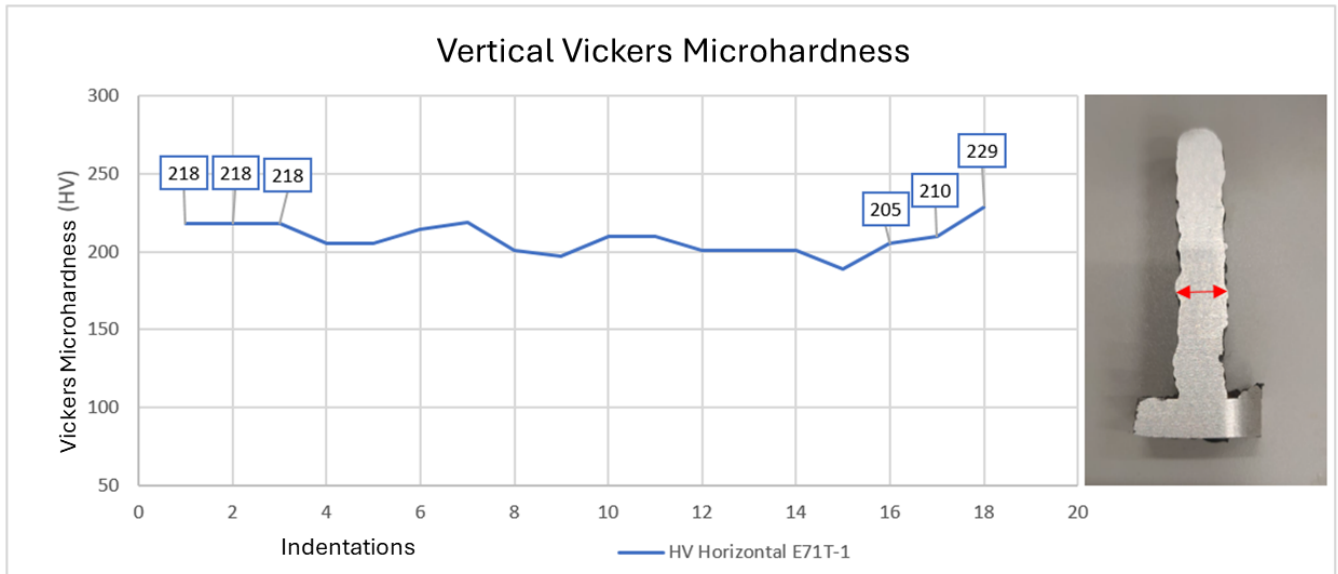


Source: From the author (2024).

The E71T-1C wire showed greater uniformity, however, the ends of the wall obtained higher measurements compared to the core, with 218 and 229 HV. However, this wire showed a different

behavior, as it obtained a reduction in hardness after the third indentation, that is, after 0.3 millimeters from the end, as shown in Figure 9.

Figure 9: Microhardness E71T-1C between walls.



Source: From the author (2024).

CONCLUSION

After metallographic evaluation, it was possible to verify that for the contact surface between the materials, there is carbon migration from the base metal to the deposited material, however, the migration layer is very close to the base, which can be eliminated by separating the printed part from the base metal.

When it comes to the microhardness evaluation, the E71T-1C wire was more influenced by the temperature at the end of the wall, with a microhardness 17 % higher than the core. For the ER70S-6 wire, the increase was 11% in the same region.

However, the E71T-1C wire maintained this increase in hardness by approximately 0.3 millimeters, while the ER70S-6 wire by 0.1 millimeters.

Thus, when evaluating the microhardness between the two wires in the deposition region, the results were 224 and 184 HV for the wires E71T-1C and ER70S-6, respectively. The increase in microhardness may be linked to the amount of manganese associated with chromium present in each material studied, since the amount of carbon for the ER70S-6 material is higher about E71T-C1, however, the microhardness values were reversed.



ACKNOWLEDGMENTS

The authors thank the University Center – UNISATC for supporting research using its laboratory structure and the Foundation for the Support of Research and Innovation of the State of Santa Catarina – FAPESC for the financial support in the purchase of equipment and supplies for research.



REFERENCES

1. Alcalde, E., & Wiltgen, F. (2018). Estudo das tecnologias em prototipagem rápida: Passado, presente e futuro. **Revista de Ciências Exatas da Universidade de Taubaté, 24*(2), 12-20.*
2. Wiltgen, F. (2019, agosto 5-7). Protótipos e prototipagem rápida aditiva sua importância no auxílio do desenvolvimento científico e tecnológico. Em **Congresso Brasileiro de Engenharia de Fabricação** (10th ed.). São Carlos: UFSCar.
3. Gibson, I., Rosen, D., & Stucker, B. (2014). **Additive manufacturing technologies: 3D printing, rapid prototyping, and direct digital manufacturing**. New York: Springer.
4. Cizenski, R. P., Daleffe, A., Ferreira, C. A., & Shaeffer, L. (2024). Manufatura aditiva na construção de peças metálicas para uso na indústria cerâmica. **Vincici, 8*(2), 515-541.*
5. Dinovitzer, M., Chen, X., Laliberte, J., Huang, X., & Frei, H. (2019). Effect of Wire and Arc Additive Manufacturing (WAAM) process parameters on bead geometry and microstructure. **Additive Manufacturing, 26**, 138-146. <https://doi.org/10.1016/j.addma.2019.02.004>
6. Kurapati, S. K., et al. (2023). Nanomaterials and nanostructures in additive manufacturing: Properties, applications, and technological challenges. **Nanotechnology-Based Additive Manufacturing: Product Design, Properties, Applications, 1**, 53-102.
7. Godec, D., et al. (2022). Introduction to additive manufacturing. Em D. Godec, J. Gonzalez-Gutierrez, A. Nordin, E. Pei, & J. Ureña Alcázar (Eds.), **A guide to additive manufacturing**. Cham: Springer. https://doi.org/10.1007/978-3-031-05863-9_1
8. Malshe, H., et al. (2015). Profile of sustainability in additive manufacturing and environmental assessment of a novel stereolithography process. Em **International Manufacturing Science and Engineering Conference**. American Society of Mechanical Engineers.
9. Vishwanatha, H. M., Rao, R., Maiya, M., Kumar, P., Gupta, N., Saxena, K., & Vijayan, V. (2023). Effects of arc current and travel speed on the processing of stainless steel via wire arc additive manufacturing (WAAM) process. **Journal of Adhesion Science and Technology, 38*(12), 2222-2239.*
10. Dong, Z., Torbati-Sarraf, H., Huang, C., Xu, K., Gu, X., Fu, C., Liu, X., & Meng, Z. (2024). Microstructure and corrosion behaviour of structural steel fabricated by wire arc additive manufacturing (WAAM). **Materials & Design, 244**.
11. American Welding Society. (2010a). **AWS A5.18/A5.18M – Specification for carbon steel electrodes and rods for gas shielded arc welding**. Miami, FL.
12. American Welding Society. (2010b). **AWS A5.1/A5.1M – Specification for carbon steel electrodes for shielded metal arc welding**. Miami, FL.
13. Freitas, B., Neto, J., Silva, R., Gusmão, A., & Freita, L. (2016). Microestrutura e microdureza do aço SAE 1020 em diferentes tratamentos térmicos. **Congresso Técnico Científico da Engenharia e da Agronomia – CONTECC'2016**. Disponível em: <https://docente.ifsc.edu.br/gianpaulo.medeiros/MaterialDidatico/Ci%C3%Aancia%20dos%20Materiais%20para%20Eng.%20E1%C3%A9trica/Aula%205%20-%20Caracteriza%C3%A7%C3%A3o%20dos%20Materiais/microestrutura%20e%20microdure>



za%20do%20a%C3%A7o%20sae%201020%20em%20diferentes%20tratamentos%20t%C3%A9rmicos.pdf>. Acesso em: 02 de julho de 2024.

14. Modenesi, P. (2011). *Soldabilidade de algumas ligas metálicas*. Universidade Federal de Minas Gerais, Departamento de Engenharia Metalúrgica e de Materiais. Disponível em: <<https://demet.eng.ufmg.br/wp-content/uploads/2012/10/soldabilidade.pdf>>. Acesso em: 03 de julho de 2024.
15. UTP. (1986). *UPT: Tecnologia da era nuclear. Curso técnico de soldas*. Edição de 1986.
16. Silva, S. (2011). *Mecanismo de trincamento de aço de microestrutura austeno-ferrítica em meio corrosivo: Estudo de caso* (p. 10). UFRJ, Rio de Janeiro. Disponível em: <<https://pantheon.ufrj.br/bitstream/11422/8905/1/monopoli10004407.pdf>>. Acesso em: 03 de julho de 2024.
17. Beltrán, J. (2019). *Influência do metal de adição e do gás de proteção na soldagem MAG de chapas de aço SAE 1020* (Monografia de Graduação em Engenharia Mecânica). Universidade Federal do Rio Grande do Sul, Porto Alegre. Disponível em: <<https://lume.ufrgs.br/bitstream/handle/10183/211333/001113947.pdf?sequence=1&isAllowed=y>>. Acesso em: 02 de julho de 2024.
18. Duarte, V., Rodrigues, T., Schell, N., Miranda, R., Oliveira, J., & Santos, T. (2020). Hot forging wire and arc additive manufacturing (HF-WAAM). *Additive Manufacturing, 35*. Disponível em: <<https://www.sciencedirect.com/science/article/pii/S2214860420305650>>. Acesso em: 02 de julho de 2024.